






## Article

# Control of an IPMC Soft Actuator Using Adaptive Full-Order Recursive Terminal Sliding Mode

Romina Zarrabi Ekbatabi <sup>1</sup>, Ke Shao <sup>2</sup>, Jasim Khawwaf <sup>1</sup>, Hai Wang <sup>3</sup>, Jinchuan Zheng <sup>1,\*</sup>, Xiaoqi Chen <sup>4</sup> and Mostafa Nikzad <sup>4</sup>

<sup>1</sup> School of Software and Electrical Engineering, Swinburne University of Technology, Hawthorn, VIC 3122, Australia; rominazarrabi@swin.edu.au (R.Z.E.); jshannanh@swin.edu.au (J.K.)

<sup>2</sup> Tsinghua Shenzhen International Graduate School, Tsinghua University, Shenzhen 518055, China; shao.ke@sz.tsinghua.edu.cn

<sup>3</sup> Discipline of Engineering and Energy, Murdoch University, Murdoch, WA 6150, Australia; hai.wang@murdoch.edu.au

<sup>4</sup> School of Engineering, Swinburne University of Technology, Hawthorn, VIC 3122, Australia; xiaoqichen@swin.edu.au (X.C.); mnikzad@swin.edu.au (M.N.)

\* Correspondence: jzheng@swin.edu.au

**Abstract:** The ionic polymer metal composite (IPMC) actuator is a kind of soft actuator that can work for underwater applications. However, IPMC actuator control suffers from high nonlinearity due to the existence of inherent creep and hysteresis phenomena. Furthermore, for underwater applications, they are highly exposed to parametric uncertainties and external disturbances due to the inherent characteristics and working environment. Those factors significantly affect the positioning accuracy and reliability of IPMC actuators. Hence, feedback control techniques are vital in the control of IPMC actuators for suppressing the system uncertainty and external disturbance. In this paper, for the first time an adaptive full-order recursive terminal sliding-mode (AFORTSM) controller is proposed for the IPMC actuator to enhance the positioning accuracy and robustness against parametric uncertainties and external disturbances. The proposed controller incorporates an adaptive algorithm with terminal sliding mode method to release the need for any prerequisite bound of the disturbance. In addition, stability analysis proves that it can guarantee the tracking error to converge to zero in finite time in the presence of uncertainty and disturbance. Experiments are carried out on the IPMC actuator to verify the practical effectiveness of the AFORTSM controller in comparison with a conventional nonsingular terminal sliding mode (NTSM) controller in terms of smaller tracking error and faster disturbance rejection.

**Keywords:** IPMC soft actuator; recursive terminal sliding mode; robust control



**Citation:** Ekbatabi, R.Z.; Shao, K.; Khawwaf, J.; Wang, H.; Zheng, J.; Chen, X.; Nikzad, M. Control of an IPMC Soft Actuator Using Adaptive Full-Order Recursive Terminal Sliding Mode. *Actuators* **2021**, *10*, 33. <https://doi.org/10.3390/act10020033>

Academic Editors: Ioan Ursu and Xinkai Chen

Received: 29 December 2020

Accepted: 14 February 2021

Published: 16 February 2021

**Publisher's Note:** MDPI stays neutral with regard to jurisdictional claims in published maps and institutional affiliations.



**Copyright:** © 2021 by the authors. Licensee MDPI, Basel, Switzerland. This article is an open access article distributed under the terms and conditions of the Creative Commons Attribution (CC BY) license (<https://creativecommons.org/licenses/by/4.0/>).

## 1. Introduction

Soft actuators are made of materials, which can deform in response to external forces and thermal stresses. Such materials can be in the form of particles, polymers, fluids, shape memory alloys (SMAs), liquid metals, hydrogels, or a combination of these [1]. Their favourable characteristics, such as low actuating voltage (<5 V), high power efficiency and biocompatibility make them suitable for soft mechatronics and robotic applications [2,3]. Among these, ionic polymer metal composite (IPMC) has attracted attention in many areas. The IPMC consists of a thin ion exchange membrane and two electrodes [4]. By applying a low electric field across these electrodes, a bending displacement can be created [5]. Conversely, an electrical signal will be produced when IPMC is mechanically deformed. In comparison with other smart materials, various desirable features, such as low driving voltage, agility, light weight, noiselessness give IPMC superiority [6]. These properties make this material suitable for diverse applications, including bio-devices, micro-pumps and sensors for measuring velocity, viscosity and blood pressure [7–12]. However, the main

challenge for the use of an IPMC actuator is to achieve accurate tracking, as the inherent nonlinearity of this material, caused by hysteresis and creep, makes its control a non-trivial task. Furthermore, other challenges also include parameter uncertainties and external disturbances imposed from the working environment along with the physio-chemical complexity of IPMC material and the lack of a universal and precise model for the IPMC system, which thus have been further investigated in the literature [13–15].

Various studies have revealed the characteristics of IPMC material and proposed different control algorithms including classic strategies such as impedance control [16]. Bhat et al. [17] designed a lead-slack controller to control an IPMC actuator dependent on a cross hybrid control system. The outcomes demonstrated the adequacy of the technique in an accurate regulation. Bandopadhyaya et al. [18] designed a PD controller to control a manipulator using an IPMC actuator. However, some studies showed that these classic strategies are not effective for such a material with highly nonlinear properties. Therefore, different adaptive control systems have been designed based on the existing models of hysteresis and creep to capture their dynamics and compensate for their changes [15,19,20]. One drawback of these control systems are that they are only suitable for short time actuation and in the absence of water. Hence, there is a need for designing a control system for underwater soft actuator with relatively long time actuation. Paddison et al. [21] worked on a procedure to quantify the wide range frequency of the overall permittivity of Nafion in water. Their outcomes demonstrate that the dielectric constant increments with adding water substance and diminishes with expanding frequency. Also, if a DC voltage is applied for adequate time, the initial deflection will change to steady state, which would rely on the backbone. This phenomenon is believed due to the overabundance concentration of water closing the cathode and its subsequent back-flux [22].

The sliding mode control (SMC) method, which is a powerful tool for control design of uncertain linear and nonlinear systems, have been applied for precise tracking control [23]. For example, the SMC method has been used not only for IPMC control but also linear springs [24], electrohydraulic systems [25] and industrial manipulators [26]. Liaw et al. proposed an improved SMC method which was used for the piezoelectric actuators to follow indicated movement trajectories [27]. Although both piezoelectric and IPMC actuators are smart materials, they have many different characteristics [28]. Wang et al. proposed an adaptive SMC controller to improve the position tracking capability of polymer actuators [29]. This research concentrated on controlling the tip of the IPMC actuators for a scope of trajectories. However, the main disadvantage of the SMC is the induced high-frequency and strong chattering behaviour along the control loop that may bring damages to the physical systems. To overcome the chattering issue, high-order sliding mode [30], super twisting algorithm [31], low-pass filtering [32], and the boundary layer techniques [33] have been proposed. However, in most of these strategies, the prior information about the upper bound of perturbation terms is required, which is often not applicable in the real world. In addition, either the control precision or the system transient performance would be degraded as a compromise. Another problem of the conventional SMC is its relatively long asymptotic convergence property. This problem can be avoided by using the recursive control structure, in which the reaching phase is eliminated while the finite-time convergence is guaranteed [34]. For instance, Tong et al. [35] proposed a recursive reaching-phase eliminated terminal sliding mode (TSM) control scheme for multi-input multi-output systems and others [36–39] have also extended the applications of TSM to a variety of systems including ground and flight vehicles. However, the main drawback of the TSM approaches is the singularity problem of the controller that limits its implementation. To address this issue, Khawwaf et al. [6] employed a nonsingular terminal sliding mode (NTSM) controller for the tracking control of IPMC actuators. Nevertheless, in most of the aforementioned methods, the signum function explicitly exists in the discontinuous control law that may degrade the control signal smoothness.

This paper aims to develop a fast-response, high-precision, and chattering-free sliding mode control scheme to enhance the robust tracking control performance of IPMC soft

actuators working underwater. To achieve this goal, an adaptive full-order recursive terminal sliding-mode (AFORTSM) controller is proposed. In this method, a new integral nonlinear hyperplane-based sliding manifold is designed by combining the NTSM with an integral terminal sliding mode (ITSM), which can lead to reduced convergence time and smaller tracking error with retained robustness. The performance of the proposed AFORTSM is then compared with the NTSM control method, which indicates that this new method eliminates the reaching phase with the help of the internal integral sliding mode and then achieves the successive finite-time convergence of the system along the dual-layer sliding surfaces. Moreover, the inherent full-order sliding mode makes the reaching control input be the integral of the signum function which is useful for suppressing control signal chattering. In addition, an adaptive control gain is proposed for the reaching law such that the need for prior knowledge of the upper bound of the uncertainty and disturbance is eliminated. In the rest of the paper, a dynamic model of the IPMC actuator with parametric uncertainty is first presented. Then, the control design procedure is elaborated. Moreover, theoretical proof is given to show that the proposed AFORTSM can guarantee the system tracking error to converge to zero in a finite time. The proposed AFORTSM control improves the tracking performance of the conventional NTSM controller in [6], which are finally verified through the experiments on a real IPMC actuator.

## 2. Plant Modelling

The experimental setup for the IPMC soft actuator working underwater is shown in Figure 1. An IPMC strip with a 3-dimensional size of 40 mm × 10 mm × 0.2 mm is submerged in a water tank. The IPMC is formed by a thin Nafion-117 membrane that is covered by two surfaces made up from platinum thin film electrodes. The deflection of the actuator tip is measured by a high-precision laser position sensor (ILD1420-10, MICRO-EPSILON) with a resolution of 0.5 µm and a range of 10 mm. In addition, a dSPACE-DS1103 rapid control prototyping system is used to implement the real-time controller for the IPMC actuator through the interface with MATLAB/Simulink on a PC. In our study, the sampling rate of the real-time controller is set as 250 Hz.

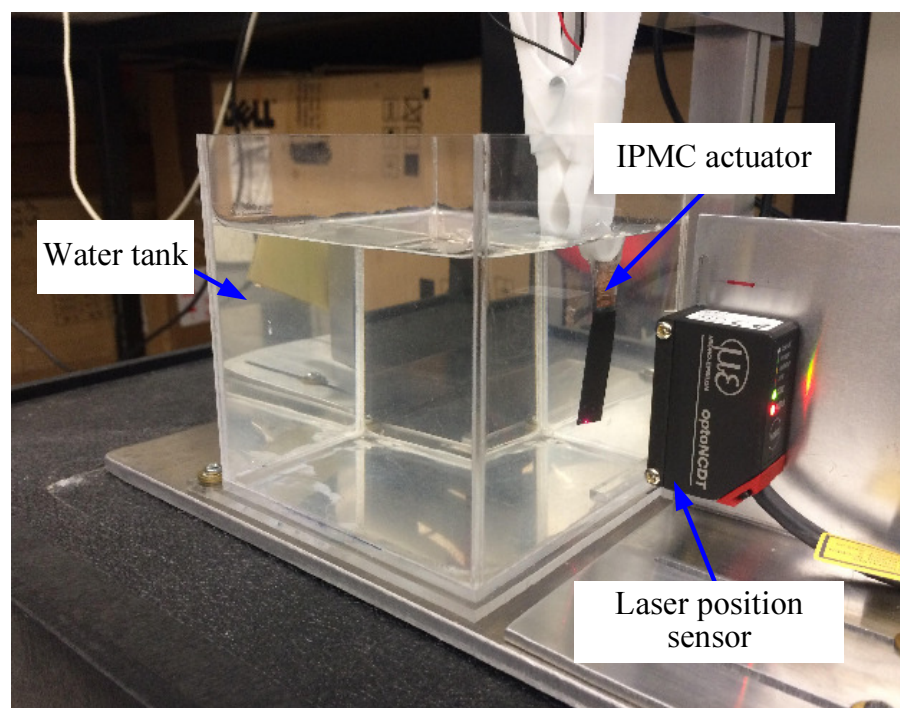


**Figure 1.** Experimental setup of an IPMC soft actuator for position tracking control underwater.

For the design of the proposed controller, a dynamic model of the IPMC actuator is required. As aforementioned, the IPMC actuator is of high nonlinearities such as creep and hysteresis that are hard to identify by a mathematical model. As such, we will consider those nonlinearities as uncertainties in this study and thus focus on a simple model for the IPMC actuator. Through an experimental identification procedure by injecting a step input voltage to the IPMC actuator and collecting the output displacement [6], we have found that the IPMC actuator can be modeled by a second-order differential equation as follows:

$$\ddot{y} = f(y) + \Delta f(y) + \tau_0 \dot{u} + \tau_1 u + d_m \quad (1)$$

where  $y$  is the IPMC displacement.  $f(y) = -a_1 \dot{y} - a_2 y$  is referred to as the nominal term related to its displacement and speed and  $\Delta f(y)$  denotes its uncertain component, respectively.  $d_m$  represents the unknown lumped uncertainty including the unmodeled nonlinear dynamics, parameter variations, external disturbance, etc.  $u$  and  $\dot{u}$  are the control voltage and its derivative, respectively.  $a_1$ ,  $a_2$ ,  $\tau_0$ , and  $\tau_1$  are the identified constants with  $\tau_0 = 0.0031$ ,  $\tau_1 = 0.0146$ ,  $a_1 = 0.4357$ , and  $a_2 = 0.1219$ , respectively. For more details on this model, the reader is referred to [6].

The control objective is to design a robust controller to achieve the fast and accurate position control of the IPMC actuator in the presence of system uncertainties. To facilitate the subsequent control design, we shall define the following variables:

$$e = y - y_d, \quad (2)$$

$$v = \tau_0 \dot{u} + \tau_1 u, \quad (3)$$

$$d_n = \Delta f(y) + d_m \quad (4)$$

where  $e$  is the position tracking error with  $y_d$  the reference command.  $v$  is the new control input to be designed, and the actual control input  $u$  can then be obtained by the filter (3).  $d_n$  represents the reformatted uncertainty. From the definition in (4), it can be seen that the derivative of  $d_n$  is associated with the displacement, velocity and acceleration of the IPMC motion. Thus, the derivative of  $d_n$  can be assumed to be bounded by

$$|\dot{d}_n| < b_0 + b_1 |y| + b_2 |\dot{y}| + b_3 |\ddot{y}| \quad (5)$$

where  $b_0$ ,  $b_1$ ,  $b_2$  and  $b_3$  are all *unknown* positive constants. Based on the preceding variables, the error dynamic equation of (1) can be obtained as

$$\ddot{e} = f(y) + v + d_n - \ddot{y}_d \quad (6)$$

which will be adopted for the control design from now on.

### 3. Control Design

In this section, an AFORTSM controller is proposed for the IPMC to track the reference command with high precision and fast speed under modelling errors, parametric uncertainties and external disturbances. To achieve this goal, a recursive integral terminal sliding mode is constructed. Based on the inherent integral sliding mode, the reaching phase is removed. Meanwhile, finite-time convergence is ensured because of the terminal sliding mode property. In addition, to handle system uncertainties, an adaptive gain is employed to approach their upper bounds in real time. Finally, selection guideline of the control parameters is discussed.

### 3.1. Construction of the AFORTSM Controller

To construct the AFORTSM controller, we first introduce the following fast non-singular terminal sliding function [40] given by

$$\sigma = \ddot{e} + c_2 \text{sig}(\dot{e})^{\alpha_2} + c_1 \text{sig}(e)^{\alpha_1} \quad (7)$$

where  $c_1, c_2$  are positive constants such that the polynomial, which corresponds to the system (7), is Hurwitz.  $\alpha_1$  and  $\alpha_2$  are the positive control parameters satisfying

$$\begin{cases} \alpha_1 \in (0, 1) \\ \alpha_2 = \frac{2\alpha_1}{1+\alpha_1} \end{cases} \quad (8)$$

and the notation  $\text{sig}(x)^a$  is a simplified expression of

$$\text{sig}(x)^a = |x|^a \text{sgn}(x) \quad (9)$$

In [41], it has been proved that when  $\sigma = 0$  in (7), the tracking error  $e$  converges to zero in a finite time  $t_\sigma$ . Next, we propose a recursive integral terminal sliding function  $s$  as follows:

$$s = \sigma + \lambda \sigma_I \quad (10)$$

where  $\sigma$  is as defined in (7), and  $\sigma_I$  is of the form

$$\dot{\sigma}_I = \text{sig}(\sigma)^\beta \quad (11)$$

with the control parameters  $\lambda > 0, 0 < \beta < 1$ . In addition, to reduce the reaching time, the initial value of the integral element  $\sigma_I$  is set as

$$\sigma_I(0) = -\lambda^{-1} \sigma(0) \quad (12)$$

Substituting (12) into (10), it is straightforward to verify that the sliding variable  $s(0) = 0$ . This implies that the control system is enforced to start on the sliding surface at the initial time such that the reaching time is removed [34]. Since the initial states of the IPMC are available in practice,  $\sigma_I(0)$  can be calculated by

$$\sigma_I(0) = -\lambda^{-1} [\ddot{e}(0) + c_2 \text{sig}(\dot{e}(0))^{\alpha_2} + c_1 \text{sig}(e(0))^{\alpha_1}] \quad (13)$$

If  $s = 0$  holds in (10), the sliding variable  $\sigma$  will converge to zero in finite time [34] given by

$$t_s = \frac{|\sigma(0)|^{1-\beta}}{\lambda(1-\beta)} \quad (14)$$

Finally, we shall give the form of the AFORTSM controller based on the recursive integral terminal sliding function. By letting  $\dot{s} = 0, \dot{d}_n = 0$ , we can obtain the following equivalent control input:

$$v_0 = -f(y) + \ddot{y}_d - c_2 \text{sig}(\dot{e})^{\alpha_2} - c_1 \text{sig}(e)^{\alpha_1} - \lambda \sigma_I \quad (15)$$

Further, a reaching control input [42] is introduced

$$v_1 = - \int_0^t (\hat{b}_0 + \hat{b}_1 |y| + \hat{b}_2 |\dot{y}| + \hat{b}_3 |\ddot{y}|) \text{sgn}(s) d\tau \quad (16)$$

where the control parameter  $\hat{b}_i$  is updated by the following adaptive law:

$$\dot{\hat{b}}_0 = \eta_0^{-1}|s| \quad (17)$$

$$\dot{\hat{b}}_1 = \eta_1^{-1}|y||s| \quad (18)$$

$$\dot{\hat{b}}_2 = \eta_2^{-1}|\dot{y}||s| \quad (19)$$

$$\dot{\hat{b}}_3 = \eta_3^{-1}|\ddot{y}||s| \quad (20)$$

with  $\eta_i > 0$  to be designed and  $\hat{b}_i(0) \geq 0$  ( $i = 0, 1, 2, 3$ ). Hence, the overall control input of the AFORTSM can be constructed as

$$\begin{aligned} v &= v_0 + v_1 \\ &= -f(y) + \ddot{y}_d - c_2 \text{sig}(\dot{e})^{\alpha_2} - c_1 \text{sig}(e)^{\alpha_1} - \lambda \sigma_I - \int_0^t (\hat{b}_0 + \hat{b}_1|y| + \hat{b}_2|\dot{y}| + \hat{b}_3|\ddot{y}|) \text{sgn}(s) d\tau \end{aligned} \quad (21)$$

### 3.2. Stability Analysis

The result for the proposed AFORTSM controller is summarized in the following theorem and stability analysis is provided.

**Lemma 1.** *Given the IPMC system in (1) and the control law (21), there exists a positive number  $b_i$  in (5) such that  $\hat{b}_i \leq b_i$  ( $i = 0, 1, 2, 3$ ) always holds.*

Proof of Lemma 1 is provided in Appendix A.

**Theorem 1.** *Consider the IPMC system in (1), then the tracking error  $e$  under the AFORTSM controller in (21) will converge from any initial condition to zero in finite time.*

**Proof.** To proceed the proof, we first obtain the derivative of the sliding function  $s$  in (10) as

$$\begin{aligned} \dot{s} &= \dot{\sigma} + \lambda \dot{\sigma}_I \\ &= \ddot{e} + c_2 \alpha_2 |\dot{e}|^{\alpha_2-1} \ddot{e} + c_1 \alpha_1 |e|^{\alpha_1-1} \dot{e} + \lambda \dot{\sigma}_I \\ &= \dot{f}(y) + \ddot{v} + \ddot{d}_n - \ddot{y}_d + c_2 \alpha_2 |\dot{e}|^{\alpha_2-1} \ddot{e} + c_1 \alpha_1 |e|^{\alpha_1-1} \dot{e} + \lambda \dot{\sigma}_I \\ &= \dot{v}_1 + \dot{d}_n \end{aligned} \quad (22)$$

Next, choose the following Lyapunov function candidate

$$V = \frac{1}{2}s^2 + \frac{1}{2} \sum_{i=0}^3 \mu_i \tilde{b}_i^2 \quad (23)$$

where  $\mu_i > 0$ ,  $\tilde{b}_i = \hat{b}_i - b_i$  ( $i = 0, 1, 2, 3$ ). Solving the derivative of (23) along the system trajectories and substituting (22) and (21) to it yields



$$\begin{aligned}
\dot{V} &= s\dot{s} + \sum_{i=0}^3 \mu_i \tilde{b}_i \dot{\tilde{b}}_i \\
&= s(\dot{v}_1 + \dot{d}_n) + \sum_{i=0}^3 \mu_i \tilde{b}_i \dot{\tilde{b}}_i \\
&= s\left(-(\hat{b}_0 + \hat{b}_1|y| + \hat{b}_2|\dot{y}| + \hat{b}_3|\ddot{y}|) \operatorname{sgn}(s) + \dot{d}_n\right) + \sum_{i=0}^3 \mu_i \tilde{b}_i \dot{\tilde{b}}_i \\
&\leq -(\hat{b}_0 + \hat{b}_1|y| + \hat{b}_2|\dot{y}| + \hat{b}_3|\ddot{y}|)|s| + |\dot{d}_n||s| + \sum_{i=0}^3 \mu_i \tilde{b}_i \dot{\tilde{b}}_i \\
&\quad -(b_0 + b_1|y| + b_2|\dot{y}| + b_3|\ddot{y}|)|s| \\
&\quad + (b_0 + b_1|y| + b_2|\dot{y}| + b_3|\ddot{y}|)|s| \\
&= -(b_0 + b_1|y| + b_2|\dot{y}| + b_3|\ddot{y}| - |\dot{d}_n|)|s| \\
&\quad + \mu_0 \eta_0^{-1} \tilde{b}_0 |s| + \mu_1 \eta_1^{-1} \tilde{b}_1 |y| |s| \\
&\quad + \mu_2 \eta_2^{-1} \tilde{b}_2 |\dot{y}| |s| + \mu_3 \eta_3^{-1} \tilde{b}_3 |\ddot{y}| |s| \\
&\quad - (\tilde{b}_0 + \tilde{b}_1|y| + \tilde{b}_2|\dot{y}| + \tilde{b}_3|\ddot{y}|)|s| \\
&= -(b_0 + b_1|y| + b_2|\dot{y}| + b_3|\ddot{y}| - |\dot{d}_n|)|s| \\
&\quad + (\mu_0 \eta_0^{-1} - 1)|s|(\hat{b}_0 - b_0) \\
&\quad + (\mu_1 \eta_1^{-1} - 1)|y||s|(\hat{b}_1 - b_1) \\
&\quad + (\mu_2 \eta_2^{-1} - 1)|\dot{y}||s|(\hat{b}_2 - b_2) \\
&\quad + (\mu_3 \eta_3^{-1} - 1)|\ddot{y}||s|(\hat{b}_3 - b_3)
\end{aligned} \tag{24}$$

From Lemma 1, we have obtained  $\hat{b}_i \leq b_i$  ( $i = 0, 1, 2, 3$ ). Then, (24) becomes

$$\begin{aligned}
\dot{V} &\leq -(b_0 + b_1|y| + b_2|\dot{y}| + b_3|\ddot{y}| - |\dot{d}_n|)|s| \\
&\quad - (\mu_0 \eta_0^{-1} - 1)|s|(\hat{b}_0 - b_0) \\
&\quad - (\mu_1 \eta_1^{-1} - 1)|y||s|(\hat{b}_1 - b_1) \\
&\quad - (\mu_2 \eta_2^{-1} - 1)|\dot{y}||s|(\hat{b}_2 - b_2) \\
&\quad - (\mu_3 \eta_3^{-1} - 1)|\ddot{y}||s|(\hat{b}_3 - b_3)
\end{aligned} \tag{25}$$

Define the following symbols

$$\begin{aligned}
\sigma_s &= b_0 + b_1|y| + b_2|\dot{y}| + b_3|\ddot{y}| - |\dot{d}_n| \\
\sigma_i &= (\mu_i \eta_i^{-1} - 1) |y^{(i)}| |s|
\end{aligned}$$

where  $i = 0, 1, 2, 3$ . It is obvious that  $\sigma_s > 0$  from (5), and for any  $\eta_i$  ( $i = 0, 1, 2, 3$ ), there exists a positive constant  $\mu_i$  such that  $\mu_i \eta_i^{-1} > 1$  that implies  $\Psi > 0$ . Then, (24) can be rewritten as

$$\begin{aligned}
\dot{V} &\leq -\sigma_s |s| - \sum_{i=0}^3 \sigma_i |\tilde{b}_i| \\
&= -\sigma_s \sqrt{2} \frac{|s|}{\sqrt{2}} - \sum_{i=0}^3 \sigma_i \sqrt{\frac{2}{\mu_i}} \sqrt{\frac{\mu_i}{2}} |\tilde{b}_i| \\
&\leq -\min \left\{ \sigma_s \sqrt{2}, \sigma_i \sqrt{\frac{2}{\mu_i}} \right\} \left( \frac{|s|}{\sqrt{2}} + \sum_{i=0}^3 \sqrt{\frac{\mu_i}{2}} |\tilde{b}_i| \right) \\
&\leq -\Psi V^{\frac{1}{2}}
\end{aligned} \tag{26}$$

where

$$\Psi = \min \left\{ \sigma_s \sqrt{2}, \sigma_i \sqrt{\frac{2}{\mu_i}} \right\} \quad (27)$$

Since there must exist a constant lower bound  $\underline{\Psi}$  for any  $\Psi > 0$  such that  $0 < \underline{\Psi} \leq \Psi$  is satisfied, the following inequality holds

$$\dot{V} \leq -\underline{\Psi} V^{\frac{1}{2}} \quad (28)$$

It can be seen that the inequality (28) satisfies the finite time stability criterion in Appendix B. Specifically,  $V$  will converge from any initial condition  $V(0)$  to zero in the finite time given by

$$t_V \leq \frac{2V^{\frac{1}{2}}(0)}{\underline{\Psi}} \quad (29)$$

which indicates that the sliding variable  $s$  and the estimation error  $\tilde{b}_i$  will both converge to zero in the finite time of (29). In addition, as in the aforementioned discussion, when  $s = 0$ ,  $\sigma$  and  $e$  will successively converge to zero in the finite time of  $t_s$  and  $t_\sigma$ , respectively. Therefore, the tracking error  $e$  will converge from any initial condition to zero in the finite time of  $t_e = t_V + t_s + t_\sigma$ .

The proof is thus completed.  $\square$

**Remark 1.** The proposed recursive terminal sliding mode (RTSM) consists of two layers of sliding functions as shown in (7) and (10). Based on the RTSM, the system moves along the sliding surfaces  $s = 0$  and then  $\sigma = 0$  and finally converges to the origin in finite time. In this sequence, each sliding surface is reached successively [43]. As given in (13),  $s(0) = 0$  can be guaranteed by selecting a certain initial value of the integral element such that the reaching phase is eliminated. Moreover, different from the conventional ISMC [44] and the adaptive SMC [13], finite-time convergence is guaranteed based on the proposed RTSM. Moreover, the value of  $V(0)$  is also decreased since  $s(0) = 0$ . As a result, the time for  $V$  to reach the origin is reduced as can be seen from (29).

**Remark 2.** Thanks to the use of a second-order sliding function in (7), full-order sliding mode can be achieved. It can be seen that the proposed reaching control input (16) is of an integral form, which means that the chattering effect caused by the signum function is softened. The full-order sliding mode property is useful to achieve both smooth and high-precision control performance for IPMC actuator without impacting its transient response. Those beneficial properties have greatly enhanced the existing methods that use NTSM or filter-based control [13,34].

**Remark 3.** In practical applications, the sliding variable  $s$  is impossible to stay at zero persistently because of the measurement noise. Instead, as indicated by (17)–(20),  $s$  will be chattering around zero, which may result in a conservatively large estimated value of  $b_i$ . To alleviate this disadvantage, a dead zone technique [45] is recommended and thus the adaptive law can be modified as follows:

$$\dot{\hat{b}}_i = \begin{cases} \eta_i^{-1} |y^{(i)}| |s|, & \text{for } |s| > \epsilon \\ 0, & \text{for } |s| \leq \epsilon \end{cases} \quad (30)$$

where  $i = 0, 1, 2, 3$ ,  $\epsilon > 0$  is a small dead zone size to be selected. From (30), it can be seen that when  $s$  is within the dead zone,  $\hat{b}_i$  will retain its present value. One can verify that when  $|s| \leq \epsilon$ , the inequality (26) still holds, i.e., the finite-time stability is still guaranteed.

### 3.3. Control Parameter Selections

In practical applications, the impacts from different factors on tracking accuracy, control signal smoothness, and robustness have to be compromised [42]. In the following, the guideline of selecting the control parameters for the proposed AFORTSM controller will be discussed and their values for the IPMC actuator control system will be given.



- (1) *Selections of  $c_i, \alpha_i$  ( $i = 1, 2$ ):* A large value of  $c_i$  or a small value of  $\alpha_i$  in (7) can lead to a faster convergence speed of tracking error along the sliding surface  $\sigma = 0$ , but unfortunately it causes an increased control input amplitude as indicated in (21). In the experiments, we select  $c_1 = 10, c_2 = 5, \alpha_1 = \frac{1}{3}$  and  $\alpha_2 = \frac{1}{2}$ .
- (2) *Selections of  $\lambda, \beta$ :* As given in (14) and (15), a larger  $\lambda$  or a smaller  $\beta$  in (10) implies a smaller bound of convergence time for  $\sigma$  but at the cost of increased control input amplitude. In addition, a larger value of  $\lambda$  will increase the amplitude of the integral element, which implies a smaller steady-state tracking error [34]. Here, we select  $\lambda = 10, \beta = 0.7$ .
- (3) *Selections of  $\eta_i$  ( $i = 0, 1, 2, 3$ ):* To achieve a fast estimation of the control gain, the values of  $\eta_i$  can be selected to be sufficiently small as indicated in (17)–(20). However, too small  $\eta_i$  may cause severer overestimation or even lead to the IPMC actuator saturation. Through some tuning in the experiments,  $\eta_0 = 0.1, \eta_1 = \eta_2 = \eta_3 = 1$  are fixed for the tests.

#### 4. Experimental Results

Experiments are carried out on the developed IPMC actuator setup as shown in Figure 1 to demonstrate the efficiency of the proposed AFORTSM controller. The reference commands under test include a single-tone sinusoidal waveform and a dual-tone sinusoidal waveform, which can be expressed as follows:

$$y_{d1} = A \sin(2\pi f t) \quad (31)$$

$$y_{d2} = A_1 \sin(2\pi f_1 t) + A_2 \sin(2\pi f_2 t) \quad (32)$$

where  $A$  denotes the amplitude and  $f$  the frequency in Hertz. Moreover, the working condition of the IPMC actuator is configured as

- Without uncertainty: IPMC actuator is fully submerged in the water;
- With uncertainty: IPMC actuator is partially (three-quarters) submerged in the water;
- With disturbance: A shock electrical signal is added onto the control input.

The configurations of all the tests, which are a combination of various reference commands with uncertainty and disturbance, are listed in Table 1.

**Table 1.** Configurations of the experimental tests.

Test	Reference	Frequency (Hz)	Amplitude (mm)	Uncertainty
1	$y_{d1}$	0.02	0.05	Without uncertainty
2	$y_{d1}$	0.01	0.05	Without uncertainty
3	$y_{d1}$	0.01	0.1	Without uncertainty
4	$y_{d2}$	0.01 and 0.05	0.03 and 0.02	Without uncertainty
5	$y_{d1}$	0.02	0.05	With uncertainty
6	$y_{d1}$	0.01	0.05	With uncertainty
7	$y_{d1}$	0.01	0.1	With uncertainty
8	0	-	-	With disturbance

To quantify the tracking control performance of the IPMC actuator, the maximum absolute tracking error ( $MAX_e$ ) as well as its root mean square ( $RMS_e$ ) are used, which is defined by the following equations:

$$MAX_e = \max_{j=1 \dots n} (|y(j) - y_d(j)|) \quad (33)$$

$$RMS_e = \sqrt{\frac{1}{n} \sum_{j=1}^n (y(j) - y_d(j))^2} \quad (34)$$

where  $n$  denotes the number of samples; and  $j$  is the sample index. In addition, we compare the performance under the proposed AFORTSM controller and the NTSM controller as previously reported in [6].

#### 4.1. Single-Tone Sinusoidal Tracking

Figures 2–4 show the experimental results of tests 1 to 3, which are tracking single-tone sinusoidal references of different amplitudes and frequencies. In comparison with the NTSM controller, the AFORTSM controller has reduced the  $MAX_e$  by more than 19% for the same single-tone sinusoidal reference and significantly improved  $RMS_e$  by more than 31%. In addition, the high-frequency chattering in the tracking error profiles under AFORTSM controller is smaller than that under NTSM controller, which indicates that the AFORTSM controller has less impact on vibrating the IPMC mechanism. However, it should be pointed that as the cost of the improved tracking accuracy, the control input amplitude under the AFORTSM controller is reasonably a bit larger than that under the NTSM controller.

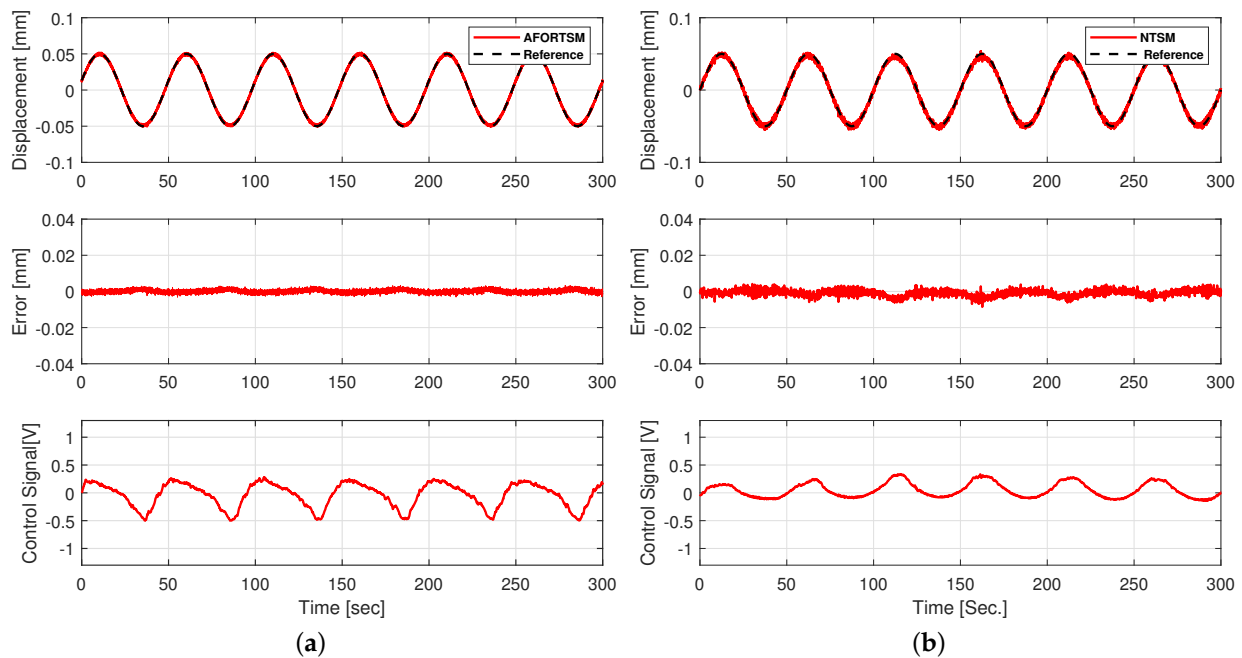


**Figure 2.** Test 1: Experimental results of AFORTSM and NTSM for tracking a single-tone sinusoidal reference without uncertainties (top: tracking profiles; middle: tracking error; bottom: control signal). (a) AFORTSM; (b) NTSM.

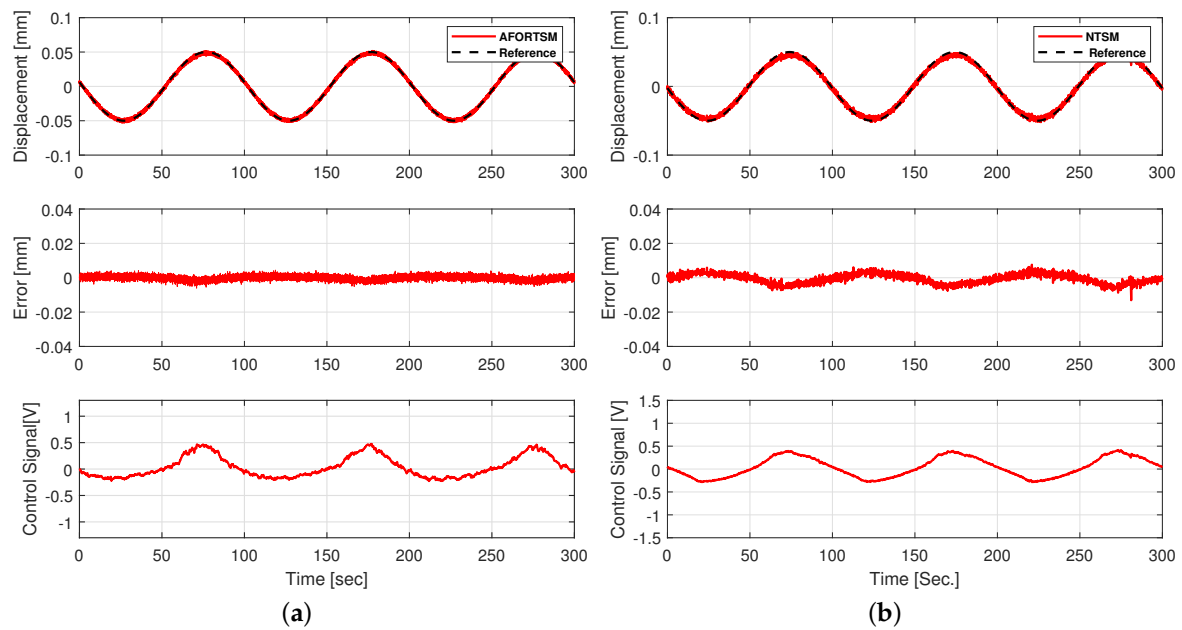


**Figure 3.** Test 2: Experimental results of AFORTSM and NTSM for tracking a single-tone sinusoidal reference without uncertainties (top: tracking profiles; middle: tracking error; bottom: control signal). (a) AFORTSM; (b) NTSM.

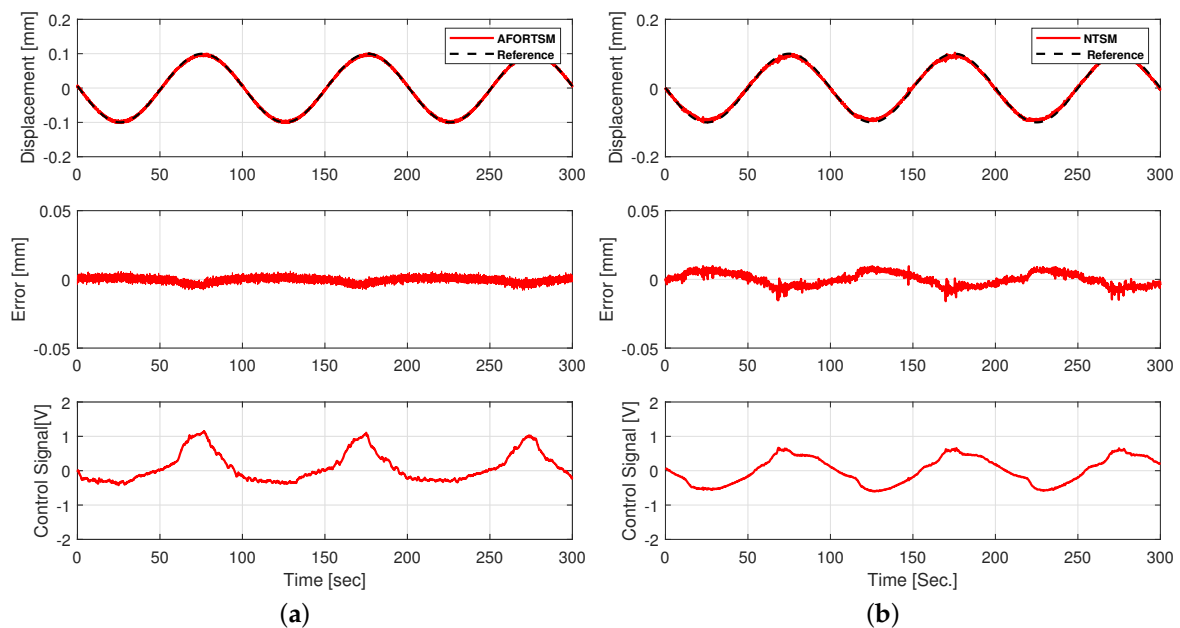


**Figure 4.** Test 3: Experimental results of AFORTSM and NTSM for tracking a single-tone sinusoidal reference without uncertainties (top: tracking profiles; middle: tracking error; bottom: control signal). (a) AFORTSM; (b) NTSM.

#### 4.2. Dual-Tone Sinusoidal Tracking

To evaluate the tracking performance for a more complex reference, test 4 is performed with a dual-tone sinusoidal reference command, whose frequencies are comprised of 0.01 and 0.05 Hz. Figure 5 presents the tracking performance of the AFORTSM and NTSM controllers for this test case. It can be seen that the  $MAX_e$  was further reduced by 32% under the AFORTSM controller, which also reduces the  $RMS_e$  by 31%. This improvement ratio is even higher than those of the single-tone sinusoidal tracking cases. Hence, this test demonstrates that the proposed AFORTSM controller can obtain smaller tracking error over a certain range of frequency bandwidth when compared with the NTSM controller.

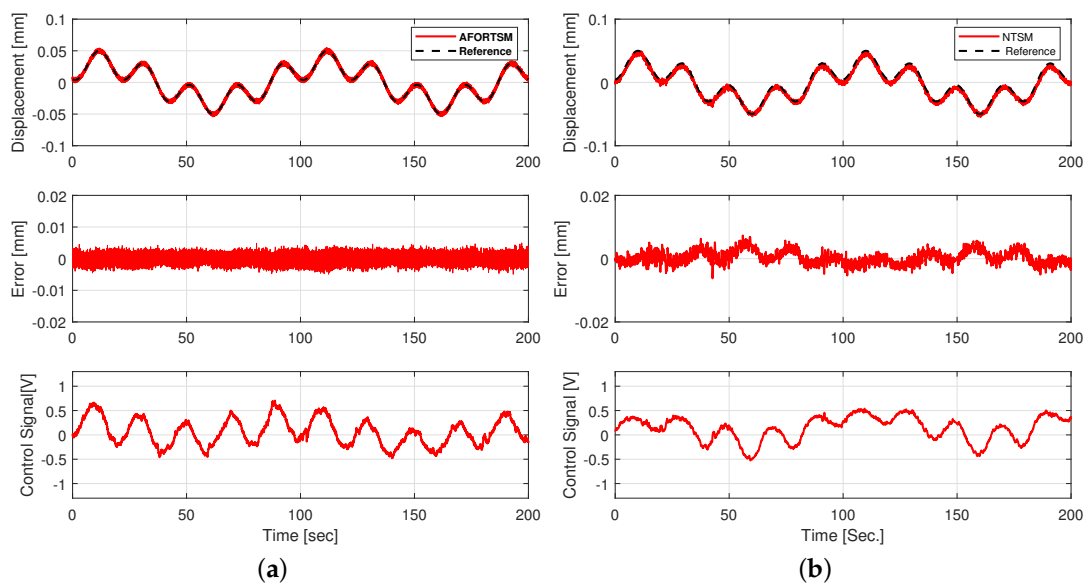


**Figure 5.** Test 4: Experimental results of AFORTSM and NTSM for tracking a dual-tone sinusoidal reference without uncertainties (top: tracking profiles; middle: tracking error; bottom: control signal). (a) AFORTSM; (b) NTSM.

#### 4.3. Robustness Verification

As aforementioned, the uncertainty in our application is regarded as the working condition of the IPMC actuator to be either fully or partially submerged in the water, under which the control system is anticipated to retain robust tracking performance. Thus, we carry out tests 5–7 with the same references as tests 1–3 except that the IPMC actuator is with uncertainty (i.e., only three-quarters submerged in the water). Similarly, Figures 6–8 show that the performance under the AFORTSM controller is still superior to that under the NTSM controller. On average, the reduction ratio of the  $MAX_e$  has been improved by approximately 33% and also the  $RMS_e$  has been improved by 64%. It is noted that the inclusion of uncertainty to the IPMC actuator has deteriorated its tracking error by about 11% on average when compared with those without uncertainty. However, this degradation is inevitable since leaving out of water will have a significant impact on the IPMC characteristics.

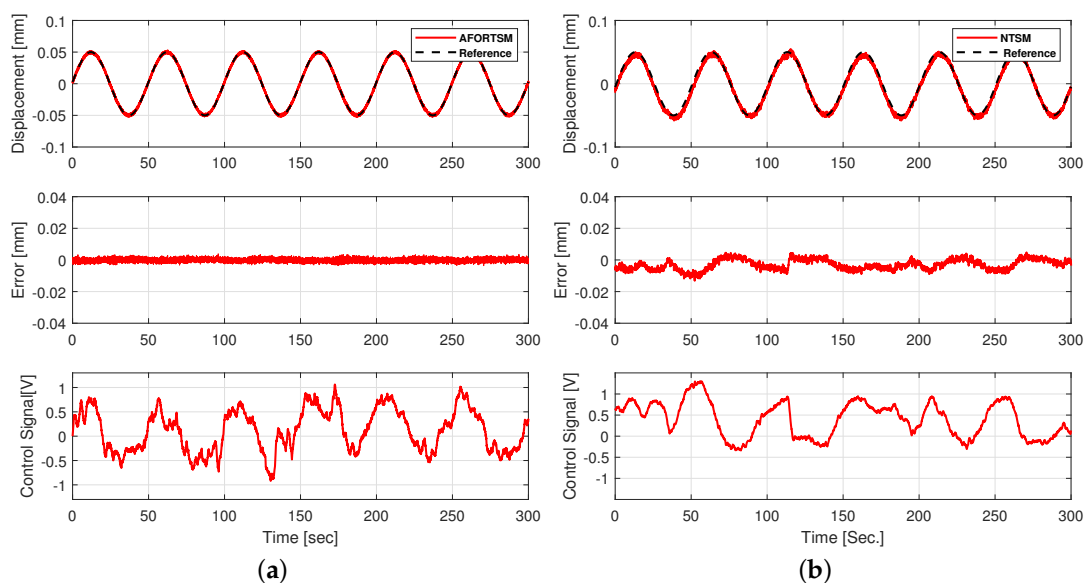


**Figure 6.** Test 5: Experimental results of AFORTSM and NTSM for tracking a single-tone sinusoidal reference with uncertainties (top: tracking profiles; middle: tracking error; bottom: control signal). (a) AFORTSM; (b) NTSM.

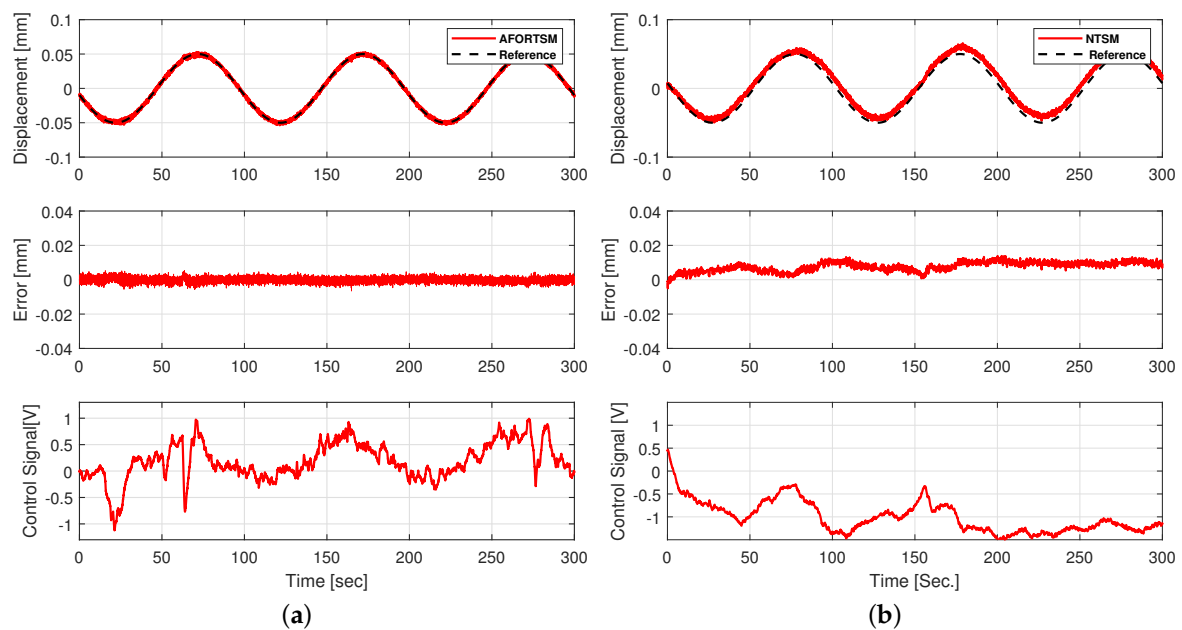


**Figure 7.** Test 6: Experimental results of AFORTSM and NTSM for tracking a single-tone sinusoidal reference with uncertainties (top: tracking profiles; middle: tracking error; bottom: control signal). (a) AFORTSM; (b) NTSM.

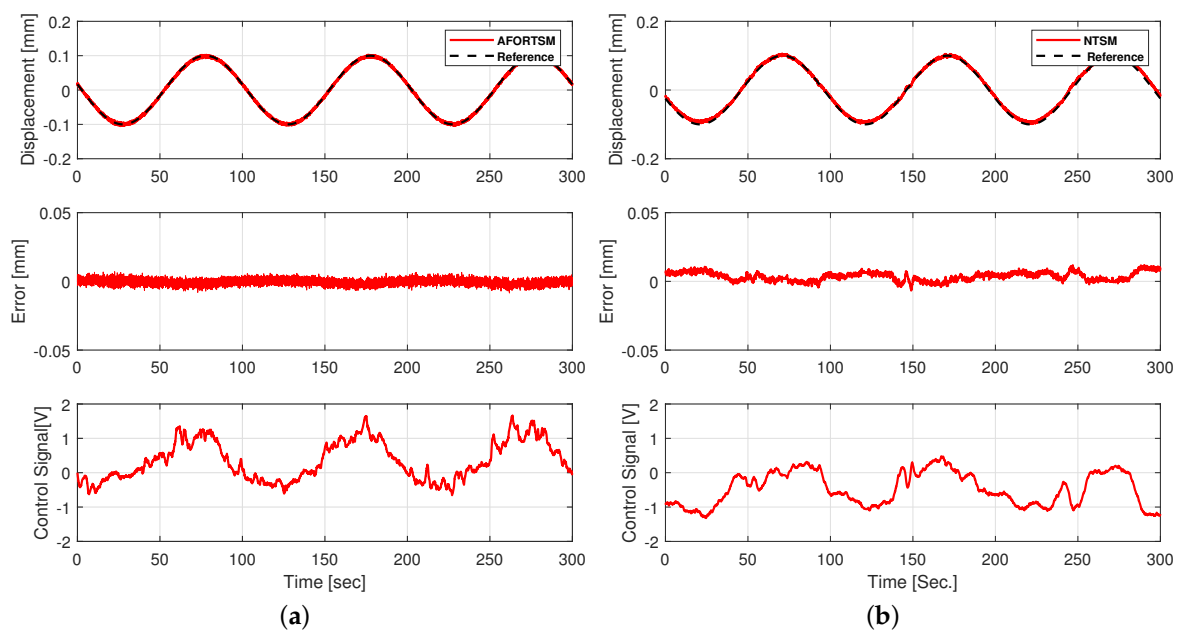


**Figure 8.** Test 7: Experimental results of AFORTSM and NTSM for tracking a single-tone sinusoidal reference with uncertainties (top: tracking profiles; middle: tracking error; bottom: control signal). (a) AFORTSM; (b) NTSM.

#### 4.4. Disturbance Rejection

The IPMC actuator may be subjected to external disturbance during operation. Hence, test 8 is conducted to evaluate its performance robustness against an electrical shock disturbance, which is artificially added to the control input. The shock disturbance has a duration of 0.5 s and an amplitude of 3 V. According to Figure 9, the AFORTSM controller has a smaller overshoot than the NTSM controller and particularly the settling time under the AFORTSM controller has been reduced by 0.5 s. This verifies the superiority of fast convergence characteristics of the proposed AFORTSM controller over the conventional NTSM controller.

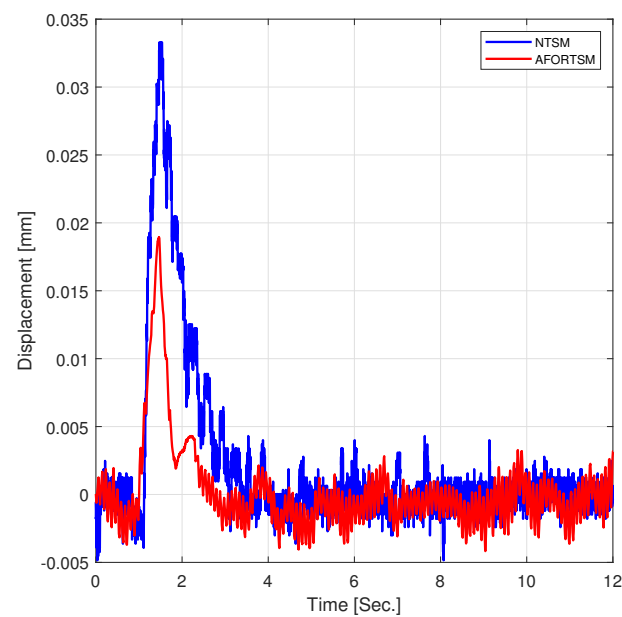


**Figure 9.** Test 8: Experimental results of shock disturbance rejection.

#### 4.5. Summary and Comparison

Table 2 summarises the performance for all test cases under the two controllers studied in this paper. According to this table, the proposed AFORTSM controller achieves superior performance compared with the NTSM controller in each case, whose improvement ratio ranges from 19% to 63% among the test cases for  $MAX_e$  and from 31% to 83% for  $RMS_e$ . Also, the comparison of the tests 5–7 (with uncertainty) to tests 1–3 (without uncertainty) shows that the proposed AFORTSM controller is significantly less sensitive to uncertainty compared with the NTSM controller. This has verified the proposed AFORTSM controller can enhance the performance robustness.

**Table 2.** Summary and comparison of experimental results.

Test	Indices	NTSM ( $\mu\text{m}$ )	AFORTSM ( $\mu\text{m}$ )	Improvement (%)
1	MAX	4.15	3.3	20
	RMS	1.99	0.73	63
2	MAX	7.61	6.1	19
	RMS	2.98	1.06	64
3	MAX	9.74	7.9	19
	RMS	4.68	1.78	61
4	MAX	7.32	5	31
	RMS	2.0	1.38	31
5	MAX	4.76	3.9	18
	RMS	4.38	0.72	83
6	MAX	13.84	6.6	52
	RMS	8.52	1.4	83
7	MAX	11.84	6.1	48
	RMS	4.85	1.56	67
8	MAX	32.45	12	63

## 5. Conclusions

The robust AFORTSM controller is proposed for the position tracking control of an IPMC soft actuator working underwater. The proposed controller has the benefits of finite-time convergence, reduced tracking error, and being chattering-free, which are owed to the proposed full-order recursive terminal sliding mode and the integral element in the reaching control law. In addition, to remove the requirement for the upper bound of



disturbance derivative during the control design, an adaptive algorithm is developed to update the control gain automatically in accordance with the varying disturbance. The proposed AFORTSM controller is verified on a real IPMC actuator and the experimental results for sinusoidal reference tracking show that it can further reduce the maximum and root mean square of the tracking errors by over 19% and 31%, respectively, in comparison with the conventional NTSM controller. Furthermore, it can achieve faster disturbance rejection, which also coincides with the theoretical property of the AFORTSM.

**Author Contributions:** Methodology, K.S., R.Z.E., J.K., H.W., J.Z.; validation, R.Z.E. and J.K.; writing original draft preparation, R.Z.E., K.S., J.Z., H.W.; resources and supervision, J.Z., X.C., and M.N.

**Funding:** This research received no external funding.

**Data Availability Statement:** The data that support the findings of this study are available from the corresponding author, J.Z., upon reasonable request.

**Conflicts of Interest:** The authors declare no conflict of interest.

## Appendix A

Given  $|s| \neq 0$ , from (17)–(20),  $\hat{b}_i$  ( $i = 0, 1, 2, 3$ ) will start to increase and then there must exist a time instance  $t_1$  such that

$$\hat{b}_0 + \hat{b}_1|y| + \hat{b}_2|\dot{y}| + \hat{b}_3|\ddot{y}| > |\dot{d}_n|$$

According to (22), from  $t = t_1$  onwards the adaptive gain will be sufficiently large to enforce the sliding variable  $s$  to decrease. Meanwhile, the adaptive gain will continue to increase until  $s = 0$  is reached in a finite time  $\Delta t$ . From then on,  $\hat{b}_i(t)$  will retain its final value of  $\hat{b}_i(t_1 + \Delta t)$ . Because of the continuity property, the value of  $\hat{b}_i(t_1 + \Delta t)$  is finite, i.e.,  $\hat{b}_i(t)$  is upper bounded. Therefore, there must exist a positive number  $b_i$  such that  $\hat{b}_i \leq b_i$  in (5) is satisfied.

This completes the proof of Lemma 1.

## Appendix B

Given the following first-order nonlinear differential inequality

$$\dot{V}(x) + \beta V^\alpha(x) \leq 0 \quad (\text{A1})$$

where the constants  $\beta > 0$ ,  $0 < \alpha < 1$ .  $V(x)$  is a positive Lyapunov function with respect to the state  $x \in R$ . Then, the function  $V(x)$  will converge from any initial condition  $V(x(0)) = V(0)$  to the origin in a finite time given by

$$t_V \leq \frac{V^{1-\alpha}(0)}{\beta(1-\alpha)}. \quad (\text{A2})$$

The derivation is referred to [46] and references therein.

## References

1. El-Atab, N.; Mishra, R.B.; Al-Modaf, F.; Joharji, L.; Alsharif, A.A.; Alamoudi, H.; Diaz, M.; Qaiser, N.; Hussain, M.M. Soft Actuators for Soft Robotic Applications: A Review. *Adv. Intell. Syst.* **2020**, *2*, 2000128. [\[CrossRef\]](#)
2. Kim, J.; Kim, J.W.; Kim, H.C.; Zhai, L.; Ko, H.U.; Muthoka, R.M. Review of soft actuator materials. *Int. J. Precis. Eng. Manuf.* **2019**, *20*, 2221–2241. [\[CrossRef\]](#)
3. Wang, J.; McDaid, A.; Sharma, R.; Aw, K.C. A compact ionic polymer metal composite (IPMC) system with inductive sensor for closed loop feedback. *Actuators* **2015**, *4*, 114–126. [\[CrossRef\]](#)
4. Truong, D.Q.; Ahn, K.K.; Nam, D.N.C.; Yoon, J.I. Identification of a nonlinear black-box model for a self-sensing polymer metal composite actuator. *Smart Mater. Struct.* **2010**, *19*, 085015. [\[CrossRef\]](#)
5. Nemat-Nasser, S.; Li, J.Y. Electromechanical response of ionic polymer-metal composites. *J. Appl. Phys.* **2000**, *87*, 3321–3331. [\[CrossRef\]](#)

6. Khawwaf, J.; Zheng, J.; Lu, R.; Al-Ghanimi, A.; Kazem, B.I.; Man, Z. Robust tracking control of an IPMC actuator using nonsingular terminal sliding mode. *Smart Mater. Struct.* **2017**, *26*, 095042. [\[CrossRef\]](#)
7. Aw, K.; McDaid, A. Bio-applications of ionic polymer metal composite transducers. *Smart Mater. Struct.* **2014**, *23*, 074005. [\[CrossRef\]](#)
8. Santos, J.; Lopes, B.; Branco, P.C. Ionic polymer–metal composite material as a diaphragm for micropump devices. *Sens. Actuators A Phys.* **2010**, *161*, 225–233. [\[CrossRef\]](#)
9. Yun, K.; Kim, W.J. System identification and microposition control of ionic polymer metal composite for three-finger gripper manipulation. *Proc. Inst. Mech. Eng. Part I J. Syst. Control Eng.* **2006**, *220*, 539–551. [\[CrossRef\]](#)
10. Konyo, M.; Konishi, Y.; Tadokoro, S.; Kishima, T. Development of velocity sensor using ionic polymer-metal composites. *Int. Soc. Opt. Photonics* **2004**, *5385*, 307–318.
11. Brunetto, P.; Fortuna, L.; Giannone, P.; Graziani, S.; Pagano, F. A small scale viscometer based on an IPMC actuator and an IPMC sensor. In Proceedings of the 2010 IEEE Instrumentation & Measurement Technology Conference Proceedings, Austin, TX, USA, 3–6 May 2010; pp. 585–589.
12. Keshavarzi, A.; Shahinpoor, M.; Kim, K.J.; Lantz, J.W. Blood pressure, pulse rate, and rhythm measurement using ionic polymer-metal composite sensors. *Int. Soc. Opt. Photonics* **1999**, *3669*, 369–376.
13. Khawwaf, J.; Zheng, J.; Chai, R.; Lu, R.; Man, Z. Adaptive microtracking control for an underwater IPMC actuator using new hyperplane-based sliding mode. *IEEE/ASME Trans. Mechatron.* **2019**, *24*, 2108–2117. [\[CrossRef\]](#)
14. Wang, J.; McDaid, A.J.; Lu, C.Z.; Aw, K.C. A compact ionic polymer-metal composite (IPMC) actuated valveless pump for drug delivery. *IEEE/ASME Trans. Mechatron.* **2016**, *22*, 196–205. [\[CrossRef\]](#)
15. Hao, L.; Li, Z. Modeling and adaptive inverse control of hysteresis and creep in ionic polymer–metal composite actuators. *Smart Mater. Struct.* **2010**, *19*, 025014. [\[CrossRef\]](#)
16. Richardson, R.C.; Levesley, M.C.; Brown, M.D.; Hawkes, J.A.; Watterson, K.; Walker, P.G. Control of ionic polymer metal composites. *IEEE/ASME Trans. Mechatron.* **2003**, *8*, 245–253. [\[CrossRef\]](#)
17. Bhat, N.; Kim, W. Precision force and position control of an ionic polymer metal composite. *Proc. Inst. Mech. Eng. Part I J. Syst. Control Eng.* **2004**, *218*, 421–432. [\[CrossRef\]](#)
18. Bandopadhyaya, D.; Bhattacharya, B.; Dutta, A. Active vibration control strategy for a single-link flexible manipulator using ionic polymer metal composite. *J. Intell. Mater. Syst. Struct.* **2008**, *19*, 487–496. [\[CrossRef\]](#)
19. Sun, Z.; Hao, L.; Chen, W.; Li, Z.; Liu, L. A novel discrete adaptive sliding-mode-like control method for ionic polymer–metal composite manipulators. *Smart Mater. Struct.* **2013**, *22*, 095027. [\[CrossRef\]](#)
20. Chen, X.; Su, C.Y. Adaptive control for ionic polymer-metal composite actuators. *IEEE Trans. Syst. Man Cybern. Syst.* **2016**, *46*, 1468–1477. [\[CrossRef\]](#)
21. Peng, J.; Zawodzinski, T.A. Describing ion exchange membrane-electrolyte interactions for high electrolyte concentrations used in electrochemical reactors. *J. Membr. Sci.* **2020**, *593*, 117340. [\[CrossRef\]](#)
22. Kamamichi, N.; Yamakita, M.; Asaka, K.; Luo, Z.W. A snake-like swimming robot using IPMC actuator/sensor. In Proceedings of the 2006 IEEE International Conference on Robotics and Automation, ICRA, Orlando, FL, USA, 15–19 May 2006; pp. 1812–1817.
23. Su, C.Y.; Wang, Q.; Chen, X.; Rakheja, S. Adaptive variable structure control of a class of nonlinear systems with unknown Prandtl-Ishlinskii hysteresis. *IEEE Trans. Autom. Control* **2005**, *50*, 2069–2074.
24. Vo, C.P.; Phan, V.D.; Nguyen, T.H.; Ahn, K.K. A compact adjustable stiffness rotary actuator based on linear springs: working principle, design, and experimental verification. *Actuators* **2020**, *9*, 141. [\[CrossRef\]](#)
25. Trinh, H.A.; Truong, H.V.A.; Ahn, K.K. Fault estimation and fault-tolerant control for the pump-controlled electrohydraulic system. *Actuators* **2020**, *9*, 132. [\[CrossRef\]](#)
26. Zhou, Z.; Wu, B. Adaptive sliding mode control of manipulators based on fuzzy random vector function links for friction compensation. *Optik* **2020**, *227*, 166055. [\[CrossRef\]](#)
27. Liaw, H.C.; Shirinzadeh, B.; Smith, J. Enhanced sliding mode motion tracking control of piezoelectric actuators. *Sens. Actuators A Phys.* **2007**, *138*, 194–202. [\[CrossRef\]](#)
28. Hao, L.; Chen, Y.; Sun, Z. The sliding mode control for different shapes and dimensions of IPMC on resisting its creep characteristics. *Smart Mater. Struct.* **2015**, *24*, 045040. [\[CrossRef\]](#)
29. Wang, X.; Alici, G.; Nguyen, C.H. Adaptive sliding mode control of tri-layer conjugated polymer actuators. *Smart Mater. Struct.* **2012**, *22*, 025004. [\[CrossRef\]](#)
30. Di Gennaro, S.; Domínguez, J.R.; Meza, M.A. Sensorless high order sliding mode control of induction motors with core loss. *IEEE Trans. Ind. Electron.* **2013**, *61*, 2678–2689. [\[CrossRef\]](#)
31. Gonzalez, T.; Moreno, J.A.; Fridman, L. Variable gain super-twisting sliding mode control. *IEEE Trans. Autom. Control* **2011**, *57*, 2100–2105. [\[CrossRef\]](#)
32. Tseng, M.L.; Chen, M.S. Chattering reduction of sliding mode control by low-pass filtering the control signal. *Asian J. Control* **2010**, *12*, 392–398. [\[CrossRef\]](#)
33. Fallaha, C.J.; Saad, M.; Kanaan, H.Y.; Al-Haddad, K. Sliding-mode robot control with exponential reaching law. *IEEE Trans. Ind. Electron.* **2010**, *58*, 600–610. [\[CrossRef\]](#)
34. Shao, K.; Zheng, J.; Huang, K.; Wang, H.; Man, Z.; Fu, M. Finite-time control of a linear motor positioner using adaptive recursive terminal sliding mode. *IEEE Trans. Ind. Electron.* **2019**, *67*, 6659–6668. [\[CrossRef\]](#)

- 
35. Tong, S.; Zhang, L.; Li, Y. Observed-based adaptive fuzzy decentralized tracking control for switched uncertain nonlinear large-scale systems with dead zones. *IEEE Trans. Syst. Man Cybern. Syst.* **2015**, *46*, 37–47. [\[CrossRef\]](#)
  36. Wang, C.H.; Huang, D.Y. A new intelligent fuzzy controller for nonlinear hysteretic electronic throttle in modern intelligent automobiles. *IEEE Trans. Ind. Electron.* **2012**, *60*, 2332–2345. [\[CrossRef\]](#)
  37. Xu, Q. Identification and compensation of piezoelectric hysteresis without modeling hysteresis inverse. *IEEE Trans. Ind. Electron.* **2012**, *60*, 3927–3937. [\[CrossRef\]](#)
  38. Tao, G.; Kokotovic, P.V. Adaptive control of plants with unknown hystereses. *IEEE Trans. Autom. Control* **1995**, *40*, 200–212. [\[CrossRef\]](#)
  39. Tan, X.; Baras, J.S. Modeling and control of hysteresis in magnetostrictive actuators. *Automatica* **2004**, *40*, 1469–1480. [\[CrossRef\]](#)
  40. Shao, K.; Zheng, J.; Wang, H.; Xu, F.; Liang, B. Recursive sliding mode control with adaptive disturbance observer for a linear motor positioner. *Mech. Syst. Signal Process.* **2020**, *146*. [\[CrossRef\]](#)
  41. Hong, Y.; Xu, Y.; Huang, J. Finite-time control for robot manipulators. *Syst. Control Lett.* **2002**, *46*, 243–253. [\[CrossRef\]](#)
  42. Deng, B.; Shao, K.; Zhao, H. Adaptive second order recursive terminal sliding mode control for a four-wheel independent steer-by-wire system. *IEEE Access* **2020**, *8*, 75936–75945. [\[CrossRef\]](#)
  43. Chiu, C.S. Derivative and integral terminal sliding mode control for a class of MIMO nonlinear systems. *Automatica* **2012**, *48*, 316–326. [\[CrossRef\]](#)
  44. Shtessel, Y.; Edwards, C.; Fridman, L.; Levant, A. *Sliding Mode Control and Observation*; Springer: New York, NY, USA, 2014.
  45. Edwards, C.; Spurgeon, S. *Sliding Mode Control: Theory and Applications*; CRC Press: Boca Raton, FL, USA, 1998.
  46. Moulay, E.; Perruquetti, W. Finite time stability and stabilization of a class of continuous systems. *J. Math. Anal. Appl.* **2006**, *323*, 1430–1443. [\[CrossRef\]](#)